PCCP

ROYAL SOCIETY OF CHEMISTRY

ARTICLE TYPE

Cite this: DOI: 10.1039/xxxxxxxxxx

Multiscale Partial Charges estimation on Graphene for neutral, doped and charged flakes†

Anastasiia Maslechko,[a] Toon Verstraelen,[b] Titus S. van Erp,[a,b] and Enrico Riccardi[a]

Received Date
Accepted Date

DOI: 10.1039/xxxxxxxxxx

www.rsc.org/journalname

The minimal-basis iterative stockholder (MBIS) and restrained electrostatic potential (RESP) methods were applied to examine the effects of edges and of nitrogen and boron dopants on the atomic partial charges of neutral and charged graphene flakes. The results provided the parameters to fit a second-order atom-condensed Kohn-Sham DFT model (ACKS2), accurately determining the partial charges, the dipole and local electric fields in large graphene flakes with negligible cost. Our approach can lead to improvements of graphene force fields in charged conditions and guide the design of media for catalytic applications.

1 Introduction

Graphene is a two-dimensional material that, since its discovery in 2004[1], got immediate and massive attention from both experimental and theoretical researchers. Since it behaves fundamentally different than ordinary three-dimensional materials, it is believed to open up completely new territories of applications.[2] In addition, the determination of its properties allowed the construction of more complex variants, such as nano-ribbons, bilayers, quantum dots, fibres, nano-coils, further increasing its possible applications. For example, graphene nano-flakes and graphene nano-ribbons are used in different electronics applications,[3] mostly due to the size controllable energy band gap. The conductance, optical properties, and the electronic structure of graphene can be exploited in exploratory electronic and optoelectronic devices.[4] Doping and defects are thus constitutive variables that selectively alter the graphene properties.[5]

Graphene variants, such as doped graphene[6], graphane (hydrogen-passivated graphene)[7,8], have also been proposed and studied, resulting in a large span of novel applications including high-performance transistor devices, energy conversion and storage components, biosensors, and photocatalysts.

One of the most promising features of the 2D material is its tunable surface properties. The interactions of O_2, N_2, CO, B_2, and H_2O molecules with graphene can, for example, be manipulated by introducing dopants or defects.[9–11] Investigations on the adsorption process of small molecules[12] such as NH_3 and NO_2,[13] benzene, and naphthalene[14] on graphene monolayers revealed the changes of partials charges and other electronic properties during the adsorption process.[15]

Most theoretical investigations on graphene carry translational periodicity of an infinite 2D sheet,[16] focusing on the properties of an ideal system. Edge effects and the role of vacancies have been shown to be determinant in the graphene behaviour.[17] For applications like electro-wetting in charged nanotubes,[18,19] electric swing,[20] electro-sorption,[21] the complex electrical properties[22] of the graphene structure and the role of its impurities, defects, edges, doping, and dipoles have to be included. In such high conductivity medium, local effects can alter the electrical properties of the whole medium, invalidating simple assumptions of uniform charge distributions.[20] The charge distribution has been shown to be determinant in adsorption processes.[15,23,24]

The present work reports on partial charge estimations in graphene based systems. We computed the charge distribution in a graphene flakes under different charge conditions and also in the presence of dopants B and N, which are known to preserve the geometrical properties of the material. Since small systems are sensitive to either the edge type or the internal structure within the carbon area, we applied a robust approach, named minimal basis iterative stockholder (MBIS),[25] which is a recent variant of the iterative Hirshfeld method.

The results have then been compared to conventional electrostatic potential fitted charges and to population analysis approaches and compared to existing ones in literature.[5,15] Evaluation of the partial charges have also been obtained by applying a physical model derived from the electronegativity equalization method. An almost immediate quantification of a large number of potential dopant positions became thus accessible. The results allow the prediction of the charge distribution on bigger size flakes that would otherwise require significant, if not even untreatable, computational efforts. The method permits computational high-throughput screenings of configurations in order to generate pre-

[a] Department of Chemistry, Norwegian University of Science and Technology, Høgskoleringen 5, 7491 Trondheim, Norway. E-mail: enrico.riccardi@ntnu.no
[b] Center for Molecular Modeling, Ghent University, Technologiepark 903, 9052 Zwijnaarde, Belgium

cisely an electric field of interest, e.g. for catalytic or electronics applications.

The paper is organized as follows. In Section 2, we briefly outline the theoretical methodologies applied for the computations, presenting also the MBIS approach. In Section 3 we report various graphene systems here considered, while the results are reported in Sections 4 and 5. Final remarks are presented in Section 6.

2 Modelling atomic partial charges

Several methods have been proposed in the literature to partition molecular properties into atomic contributions. Most of them estimate atomic charges, as a post-processing analysis after the computation of the electronic structure, e.g. with density functional theory. When it comes to post-processing, there are two major distinct families of methods: those based on the molecular electrostatic potential and those based on the electronic density or density matrix. In this work, we selected a method from each category: restrained electrostatic potential (RESP)[26] fitted charges and minimal-basis iterative stockholder (MBIS)[25], respectively. Furthermore, in order to reduce the computational expense of the DFT calculation, a electronegativity equilibration model (EEM)[27] has been considered, in particular, the atom-condensed Kohn-Sham method approximated to the second order (ACKS2).[28,29]

Electrostatic potential (ESP) fitted charges are conventionally estimated for the development of force field models because they optimally reproduce the molecular ESP by construction.[30] The basic idea of is to perform a least-squares minimization of the atomic charges to reproduce the DFT electrostatic potential at chosen grid points and different schemes exist to select these grid points, which usually lie closely to the molecular van der Waals surface. Despite it's straightforward benefits, ESP fitted charges also have some serious drawbacks. In bulky molecules, a change in atomic charge of a buried atom can be compensated by a corresponding change in surface atoms with a negligible change in the ESP. Hence, such variations in charge cannot be observed with ESP fitted charges methods. Secondly, ESP-fitted charges depend significantly on the geometry, troubling their application to flexible molecules. Both limitations sometimes result in atomic charges with unreasonably large magnitude. Such excessive charges can be treated symptomatically with hyperbolic restraints as in the restrained ESP (RESP) method.[26] Since the graphene flakes in this work are relatively rigid and all atoms are accessible from the van der Waals surface, the weaknesses of ESP fitted charges are expected to have a small impact. However, as discussed later on, our results do not fully comply with this expectation.

More recently, electron density-based methods were advocated for force-field development purposes. The basic idea is to divide the molecular electron density into atomic partitions. Each density partition integrates to the atomic population, which together with the nuclear charge yield the atomic partial charge: $q_A = Z_A - N_A$. Even though the quantum theory of atoms in molecules (QTAIM) is conceptually very attractive, it has slowly converging atomic multipoles, such that atomic charges alone cannot reproduce electrostatic interactions. Hirshfeld partitioning, and in particular its modern variants, exhibit a much faster convergence of the atomic multipole expansions. This advantage spurred the development of new variants of the Hirshfeld method, which satisfactory approximate electrostatic potentials (comparable to ESP fitted charges)[25] and also reproduce electrostatic interactions accurately (better than ESP-fitted charges).[25] Other main advantages of electron density-based methods are the low sensitivity to conformational changes and the absence of any issues with buried atoms. The electron density-based method used here is the minimal-basis iterative stockholder (MBIS) method.[25]

In this work, we will also test to what extent atomic partial charges in graphene flakes can be reproduced with fluctuating-charge methods, which are computationally orders of magnitude cheaper than density functional theory (DFT) calculations and therefore potentially applicable to larger flakes. Here, the basic idea is to minimize an approximate electronic energy as function of the atomic charges, with a constraint on the net molecular charge. Besides the interatomic distances, empirical parameters appear in the energy expression, which must first be calibrated before a fluctuating charge-model can be applied. The simplest example of this concept is the electronegativity equalization method (EEM), which proposes a quadratic energy expression:

$$E_{\mathrm{EEM}} = \sum_{i=1}^{N} \left(\chi_i q_i + \frac{1}{2}\eta_i q_i^2 + \sum_{j=i+1}^{N} \frac{q_i q_j}{4\pi\varepsilon_0 R_{ij}} \right) \tag{1}$$

where N is the number of atoms, χ_i and η_i are empirical atomic parameters and R_{ij} is the distance between nuclei of atoms i and j.

While it was shown many times that EEM and similar models can reproduce atomic charges derived from DFT calculations reasonably well,[31] this simple formalism has a few important restrictions. The most problematic issue is that the EEM dipole polarizability scales with the third power of the system size, which is formally incorrect for dielectric systems.[32] This was addressed in the split-charge equilibration[33] and the atom-condensed Kohn-Sham (ACKS2) method.[28,29] Formally, ACKS2 is a simple extension of EEM, with one extra energy term related to the electronic kinetic energy: $E_{\mathrm{ACKS2}} = E_{\mathrm{EEM}} + T_{\mathrm{ACKS2}}$ with

$$T_{\mathrm{ACKS2}} = \max_{u_i} \sum_{i=1}^{N} \left((q_i - q_i^0)u_i + \sum_{j>i}^{N} X_{ij} u_i u_j \right) \tag{2}$$

where u_i are changes in the atomic Kohn-Sham potential relative to the isolated atom i. For a given set of partial charges q_i, the set of u_i has to be found that maximizes T_{ACKS2} under constraint that the sum is zero: $\sum_i u_i = 0$. The reference charge q_i^0 is a fixed integer charge (similar to oxidation state). The terms X_{ij} are the elements of the charge-charge response matrix of non-interacting fermions in a fixed effective potential. It can be derived from a Kohn-Sham DFT calculation and may have a complicated geometry dependence.

For large inter-atomic distances, off-diagonal elements X_{ij} decay exponentially with distance, which we will use as model for

all distances:

$$X_{ij} \approx X_{ij}^{0} \exp(-R_{ij}/\tau_{ij}) \text{ , for } i \neq j \quad (3)$$

where X_{ij}^{0} and τ_{ij} are empirical atom-pair parameters. The diagonal elements X_{ii} are such that the sum of all elements over one row (or column) is zero (This sum rule is related to fact the the number of electrons is fixed). In EEM and ACKS2, empirical parameters are associated with (pairs of) chemical elements, instead of individual atoms, to limit the number of independent parameters.

3 Methodology

3.1 Classification of graphene flakes

We consider two types of flakes depicted in Fig. 1. They resemble graphene material and are still computationally treatable, with a symmetrical structures that facilitates their analysis. Type I consists of 3 geometrically identical graphene flakes of 53 atoms in which the central atom is either substituted by boron, nitrogen or just carbon (undoped). Note, that one carbon on the edge of the type-I flake is bonded with two hydrogens to fulfil the requirement that each carbon or its substituent (N or B) possess four valence electrons. The system is symmetrical around the axis drawn in Fig. 2. Type II involves a heterodoped graphene flake consisting of 84 atoms in which the dopants (B and N, in blue and pink in Fig. 1b are located in the core area of the system. Each system type has been characterized in its neutral state (zero net charge). System type I has also been studied in its positively and negatively charged state (overall charge equal $+1e$ and $-1e$, respectively).

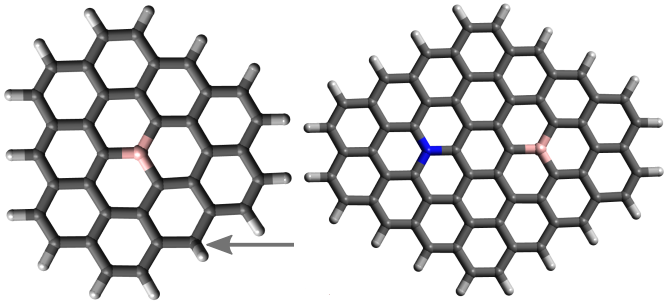

(a) (b)

Fig. 1 Graphene flakes. (a) type I system; (b) type II system. The arrow indicates the CH_2 group.

To facilitate the presentation of our results, we divided the carbon atoms in the type I system into regions. Each region is defined accounting for the network-geometry and distance from the central atom. Note that the properties of the atoms has been averaged in each region only in the geometrical descriptions, while the partial charges has been reported for each individual atom. The label "Z" indicates the central atom which can be either carbon, nitrogen or boron. The other carbon atoms have been labelled C_A, C_B, C_C, C_D, C_E, C_F, C_G, C_I according to their distance to the flake's centre, as shown in Fig. 2. Note that C_E and C_F carbons have the same distance to the centre in an ideal honey-comb structure, but are still geometrically distinct within the network. C_E is connected with hydrogen(s), while C_F is only connected to carbons. The edge-atoms are all hydrogens and are labelled "H".

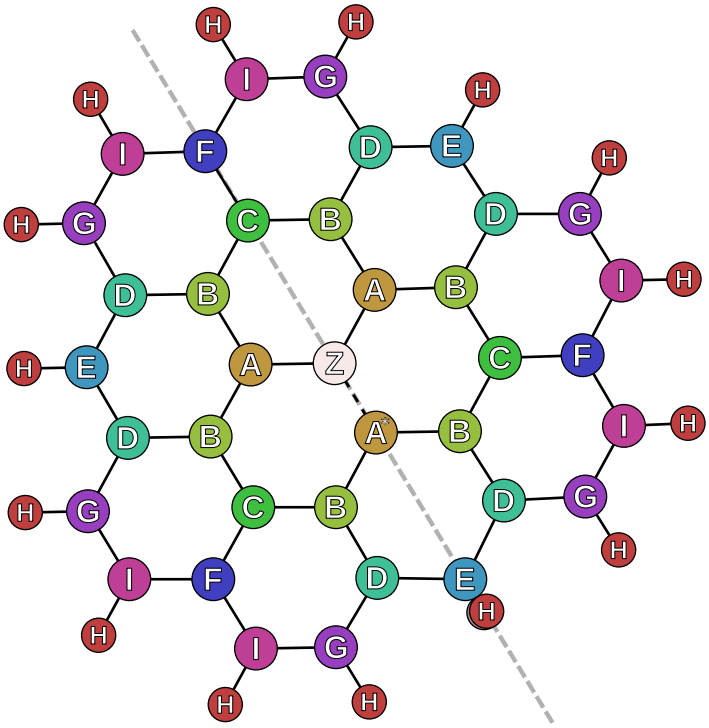

Fig. 2 Type I system, coloured by the groups. The Z atom is the centre of the graphene flake, and it can be, depending of the case, constituted by carbon, boron, or nitrogen. The labels A, B, C, D, E, F, G, I refers the C_A, C_B, C_C, C_D, C_E, C_F, C_G, C_I carbons, respectively. The group H indicates the hydrogens. The dashed line indicates the main axis of symmetry of the graphene flake.

3.2 Electronic structure calculations

Two kinds of basis sets have been compared in the systems: Pople style basis set 6-31+G(2df,p) [34] and Def2TZVP from Ahlrichs and co-workers. [35] All geometry optimizations and electron densities were calculated using the unrestricted wB97XD [36] functional as implemented in Gaussian09 code. [37] In section 4 we report only on the Def2TZVP results. These are the most relevant, since we intend to develop an approach for systems with many metal-centred atoms, which are significantly faster with Def2TZVP in comparison with 6-31+G(2df,p). The latter basis set, containing diffuse functions, results in differences only on the third digit of the values for the partial charges as can be seen in the supplementary materials.

The DFT electron densities were used as input for the computation of MBIS charges with the open-source HORTON program. [38] HORTON is a computational platform to experiment with non-standard methods for the quantum many-body problem. This package also contains several methods to post-process wavefunctions obtained with other quantum chemistry programs, such as Gaussian09. RESP calculations were performed using an online tool, the RESP ESP charge Derive (RED) Server, designed to automatically derive RESP and ESP charges [39] via cloud computing.

ACKS2 Parameter	Value
χ_H [eV]	6.6
χ_B [eV]	0.0
χ_C [eV]	14.9
χ_N [eV]	25.5
$\eta_H = \eta_B = \eta_C = \eta_N$ [eV]	11.4
X^0_{HH} [a.u.]	0.65
$X^0_{HB} = X^0_{HC} = X^0_{HN}$ [a.u.]	0.7
$X^0_{BB} = X^0_{CC} = X^0_{NN} = X^0_{BC} = X^0_{CN} = X^0_{NB}$ [a.u.]	1.5
τ_{HH} [Å]	0.6
$\tau_{HB} = \tau_{HC} = \tau_{HN}$ [Å]	1.0
$\tau_{BB} = \tau_{CC} = \tau_{NN} = \tau_{BC} = \tau_{CN} = \tau_{NB}$ [Å]	1.0

Table 1 ACKS2 parameters for doped graphene flakes

3.3 Approximate partial charges via ACKS2 method

We derived the ACKS2 model parameters from the MBIS charge distributions of three type I flakes: neutral without dopant, anionic with boron dopant and cationic with nitrogen dopant. In this way, both the B and N dopants contribute 6 electrons to the graphene flake, just like the substituted carbon atom. Under these conditions, the differences in charge distributions can be modelled as a linear response of the electron density to a perturbation of the external field, namely an alchemical change of the carbon nucleus. ACKS2, which is essentially an electronic linear response model, is henceforth a good candidate to estimate partial charges in a computational efficient way.

The three systems contain a relatively small amount of data to fit the ACKS2 parameters. Therefore, the X^0_{ij} and τ_{ij} parameters were not fitted to atomic charges. Instead they were estimated using the MBIS partitioning of the non-interacting response matrix. Furthermore, the reference charges have been fixed *a priori*: $q^0_H = q^0_C = 0$, $q^0_B = -1\,e$ and $q^0_N = 1\,e$, which is in line with the contribution of 6 electrons for elements B, C and N. For the remaining parameters, χ_i and η_i, the weighted least-squares error between MBIS and ACKS2 charges has been minimized. The B and N charge is given a ten-fold increased weight due to its relative importance in the present work. In this optimization, all hardness parameters were constrained to the same value, while each element has its specific electronegativity parameter. Because the least-squares procedure can only determine the electronegativity parameters up to a constant shift, the boron electronegativity is assumed as the zero reference (An increment of all electronegativity parameters with the same shift would not change the results). All ACKS2 parameters are given in Table 1.

The weighted root-mean-square deviation between the ACKS2 and MBIS charges of the three type I flakes, using the same weights as in least-squares error, is $0.052\,e$ which is relatively small compared to the absolute values of the charges. When applying the ACKS2 model with the same parameters to the type II flake, the weighted RMSD is $0.085\,e$, showing that the model is transferable to doped flakes that were not used to fit the parameters.

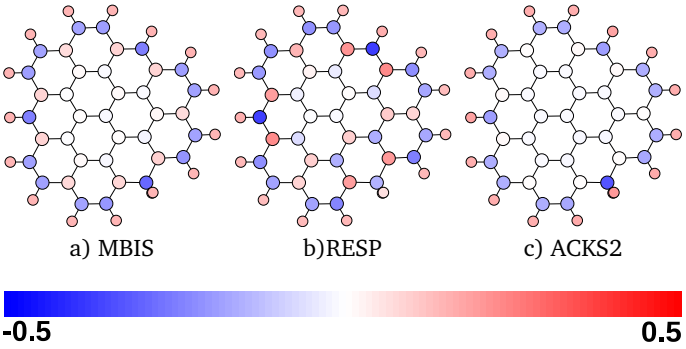

Fig. 3 Charge distribution for the neutral undoped type I system estimated via a) MBIS, b) RESP and c) ACKS2.

4 Partial charges and charge-shifts

4.1 Atomic charges of neutral undoped Graphene Flakes

Once a structural description of type I flakes has been provided, focus can be directed towards the electrostatic properties of the flakes. In particular, we are interested in the effects that the dopants and the edges have on the redistribution of the partial charges. As aforementioned, we computed such charges with the MBIS method and compared its results with the RESP method. The partial charges obtained by the ACKS2 model are also presented.

Fig. 3 provides an immediate visual quantification of the partial charge distribution computed with MBIS, RESP and ACKS2 for the neutral undoped graphene flake. MBIS and ACKS2 approaches describe the central atoms, Z, C_A, C_B and C_C mostly as neutral. RESP predicts instead a different polarization for the atoms C_A, C_B and C_C. Moreover, the atomic charges of C_D carbons on Fig. 3b are higher than the ones of the external hydrogens. This is a unreasonable overcharge that we consider as a methodological artefact.

Our findings for this base system are in reasonable agreement with the work of 5 with respect to charges' magnitudes and the oscillatory behaviour. Still, Benerjee[5] considered Mulliken population approach, which is less precise and highly sensitive to the basis set used. Our results slightly differ from the findings of Jenness et al.[15] for coronene based systems. They reported partial charges on the flakes' edge hydrogens of +0.10 (versus ours +0.15) and -0.07 for the connected carbons (versus ours -0.18). These differences are not surprising given the different nature of their systems. Coronene systems are highly symmetrical and have a hole in the centre, while the flakes considered here are centred around a carbon or dopant, and are slightly less symmetrical (CH_2 group, see Fig. 1)

The three methods are further mostly consistent with respect to the charge gradient present at the edges of the graphene flake: the hydrogen and the outermost carbons have similar charges. The internal atom groups, instead, resulted in different charges depending on the method. MBIS predicts a negative polarization of the outer carbon atom region (C_E, C_G and C_I) followed by a positive carbon atom region C_F and C_D. The polarization of the latter region is missed by ACKS2, where the atomic charges (Fig. 3c) are only polarized at the edges.

4.2 Partial charges of doped isoelectric graphene flakes

The doped type I graphene flakes have been investigated in two different induced charge conditions: (i) the N-dopant deprived of an electron, resulting in an overall charge $+1e$, and (ii) the B-dopant with an additional electron, resulting in an overall charge $-1e$. These dopants are isoelectric with the undoped neutral graphene flake which is an requirement for the ACKS2 method, reported in section 3.3. Hence, this set of flakes allows the assessment of the partial charges using the different methods (RESP, MBIS, ACKS2).

Fig. 4 reports the partial charge distributions obtained from MBIS, RESP and ACKS2 for the doped and charged systems. The B doped systems with a $-1e$ overall charge (Figs. 4a, b, c) shows consistent negative charges located around the positive centre and at the edges (carbon atoms C_F C_G, C_I). The remaining regions are either neutral or positive. Hence, the three methods report similar trends with only some discrepancies in the magnitude of the charges.

Figs. 4d, e, and f for the N doped, $+1e$ charged graphene flakes, indicate a different scenario. The partial charges computed via RESP, Fig. 4e, on the middle N atom appears excessively positively charged. MBIS-derived charges, Fig. 4d, shows instead a reasonable polarity of the central N atom and of its surrounding carbons. The hydrogens appear to affect only the edges groups C_D and C_F. In general, ACKS2 demonstrates a physically consistent distribution with MBIS charges, but slightly underestimates the delocalization of pi-bonds, predicting slightly more localized response to the presence of dopants (dielectric character). RESP asserts that the flakes edges can induce a change of polarity of the dopant, attributing a positive atomic charge to the central N atom in the $+1e$ case (Figs. 4e). RESP therefore appears to overestimate the effect of the edges and apparently fails to capture the influence of the dopants on the flake.

It is worth noting that the number of atoms at the edges, in a flake, is larger then the number of core atoms. For this type of systems, a high accuracy in the computation of partial charges is necessary to discriminate the role of the edges from the effects of the doped atoms. Therefore, it is encouraging that the ACKS2 charges mimic the targeted MBIS partial charges with a significant lower computational effort. For this reason, in the forthcoming analysis we will focus on MBIS and ACKS2.

4.3 MBIS partial charges type I flakes

The partial charge distribution of the graphene flakes in the uncharged and charged state, with and without the dopants, are combined in Fig. 5 (and reported in the supplementary information, Tables 10-18). Fig. 5b evidences that the undoped neutral graphene flake has a mostly neutral core while the edges hydrogens are positively charged. The hydrogens induce negative partial charges to the adjacent carbons, and a small positive charge to the next-nearest neighbours. Adding or removing electrons in the undoped graphene flake, (Fig. 5a and c) induces only small perturbations, mostly at the edges. The central atoms (groups Z, C_A, C_B, C_C) shows, together, a sort of neutral entity in all the different charged states ($-1e$, $0e$, $+1e$).

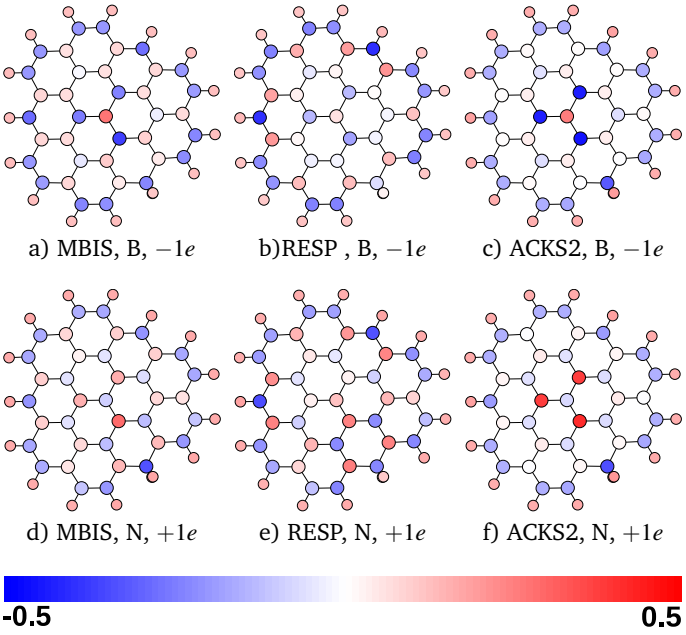

Fig. 4 Atomic charges for type I system obtained using MBIS (a, d), RESP (b, e) and ACKS2 (c, f): the first row (a, b, c) represents a single B-doped flake with a total charge $-1e$, on the bottom row (d, e, f) there are single N-doped flakes with an overall charge $+1e$.

Comparing Figs. 5b, e, and h, it is noticeable that the dopant B holds a relatively large partial charge with respect to N and C for the neutral cases. Figs. 5d-i, show the relative effects of B and N dopants for the charged cases. Both B and N dopants induce an opposite in sign partial charge in the neighbour atom type C_A (except the C along the symmetry axis in the N, $-1e$ case 5g). Surrounding atoms show a damped oscillatory trends as function of the distance from the centre. From atom type C_D to the outermost hydrogen layers minor differences with respect with the undoped graphene flake can be observed. While B has a positive partial charge, and N negative, the first induces a larger partial charge in the neighbouring carbons.The atoms in group C_A bear most of the overall charge. Atoms in groups C_D, C_E, C_F, C_G, and C_I instead, have partial charges mostly induced by the edges while the carbon atoms in groups C_E, C_F, C_G and C_I experiences most of the overall deviation. Hydrogens at the edges, therefore, have only a modest influence on the graphene flake core, confirming that the finite size of the flake is large enough to formulate generic conclusions about the effect of doping. A complete quantification can be found in the Supporting Information. In the work of Zhou et al.,[40] values for the partial charges of the dopants are reported: +0.60 for B and -0.26 for N. We obtained valued of +0.42 for B and -0.14 for N. While we note that the studied system has differences, we lack a sufficient description Zhou et al.'s methodology to replicate their findings.

4.4 MBIS charge-shift for type I electron addition/removal

We are interested, in the present work, to study the graphene flake's response to electron loading and removal. To describe the response, we visualize the condensed Fukui functions in Fig. 6 using the *response of molecular fragment approach*, i.e. the change

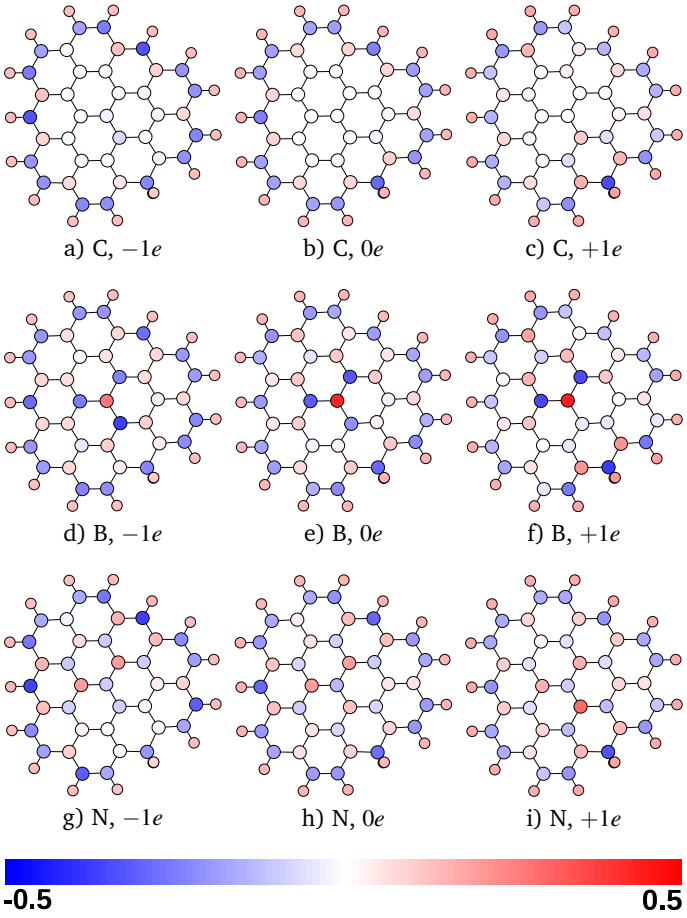

Fig. 5 Atomic charges computed via MBIS for type I system: the first row, panels a, b and c, represents the flake without any dopant, the second row, panels d, e and f, reports on the B-doped flakes, on the bottom row, panels g, h and i, the N-doped flakes. The left column reports $-1e$ charged flakes, panels a, d and g, the central column the neutral flakes, panels b, e and h and the right column $+1e$ flakes, panels c, f and i. Further details are reported in Tables 10-18 of the supplementary information.

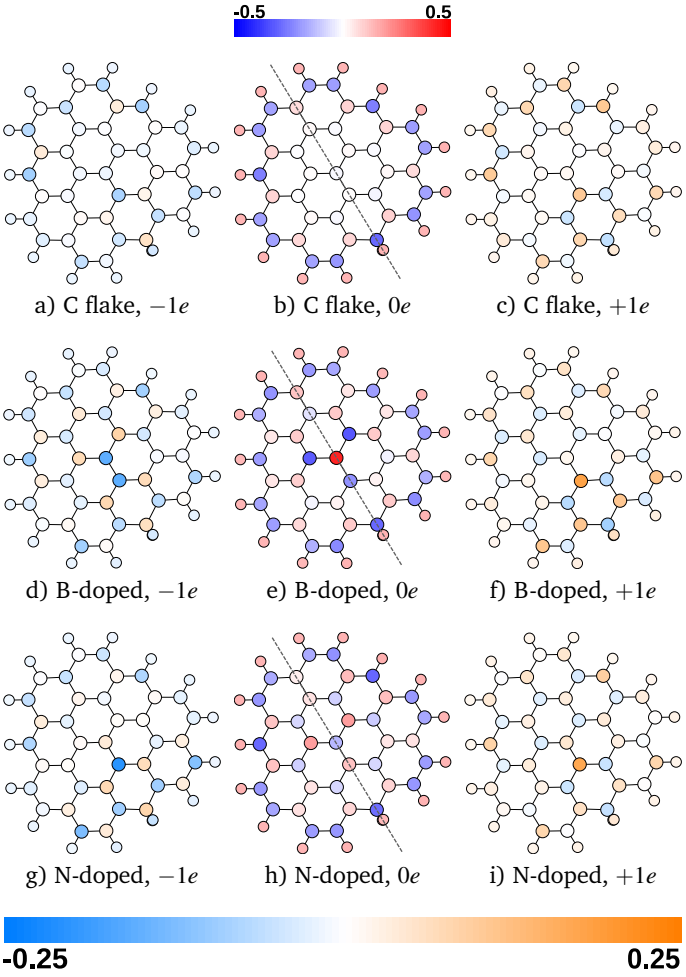

Fig. 6 Graphene flakes atomic charge-shifts for the adding/removal of $-1e$ in respect to their relative neutral cases. The left and right panels show the differences between partial charges of flakes with a net charge and that of a neutral flake (condensed Fukui functions). The neutral $0e$ case is reported in the central panels b, e and h as a reference, where in colours blue to red scale the magnitude of the partial charges is shown. The left column, panels a, d and g reports the $-1e$ cases while the right column reports the $+1e$ cases, panels c, f and i. In the latter columns the azure to orange scale indicates the magnitude of the charge-shifts.

in partial charges relative to the neutral case shown in the central column of the figure.[41] The first column refers to the addition of an electron, while the latter the removal of an electron. Figs. 6b, e, and h show again the absolute charge distribution of the neutral undoped, B-doped and N-doped flakes to facilitate the visual description.

The added negative charge to the undoped graphene flake, reported in Fig. 6a, redistributes mostly along the outer carbons of the flake, increasing their negative charge. Depriving the graphene flake by one electron, $+1e$ case described in Fig. 6c, also affects mostly the outer carbons. In both the positive and negative cases the graphene core is only modestly affected by the loaded charges.

In the presence of B-dopant with an added electron, $-1e$ case as shown in Fig. 6d, the central atom acquires most of the electron charge. Interestingly, two adjacent carbons increase their partial charges. Despite the collective effect of the hydrogens and carbons at the edges, the dopant is able to confine most of the added charge. Considering the number of the edge hydrogens, it is remarkable that a single dopant is able to dominate the charge redistribution. When removing an electron from the flake in the presence of B-dopant, $+1e$ case as showed in Fig. 6f, the edges dominate the flake response. The dopant partial charge seemed unaffected.

In the presence of N-dopant with an added electron, $-1e$ case as shown in Fig. 6g, the partial charges redistributes mostly at the flake edges. A consequent minor polarization of the adjacent carbon can also be observed. When removing, instead, an electron, $+1e$ case as shown in Fig. 6i, the edge and the dopants partial charges show a comparable increasing trend.

4.5 Partial charges and dipole moment for the neutral heterodoped type II flake

The partial charges for heterodoped graphene flakes of type II, reported in Fig. 1, have been determined via MBIS and ACKS2

with the parameters set previously obtained from type I graphene flakes. In Fig. 7, we present the results obtained; further quantitative details can be found in the supplementary information (Table 19).

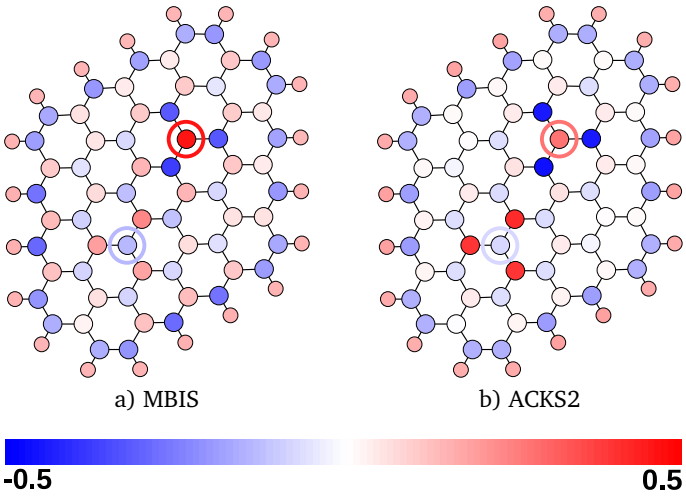

Fig. 7 Partial charges derived for system type II graphene flake using MBIS (a) and ACKS2 (b) approaches. In the red circles, the B-dopant atom and in the blue circle, the N-dopant atom are highlighted. The systems total charge is equal zero.

It can be first noted that MBIS and ACKS2 estimated partial charges are in good agreement. The dopants locate mostly the partial charges in the flake (B positive, N negative) and initiate a sort of polarization of the carbon atoms around the flake that extends to the edges. The presence of the dopants seems to increase the oscillatory behaviours of the different layers of carbons. This effect suggests that different positions of the dopants can lead to completely different electronic properties of the flake. While this phenomena is of certain interest, its computational complexity and large variety of determinant degrees of freedom require further and dedicate studies that go beyond the purpose of the present work.

5 Geometry deformations and local electric field

5.1 Geometrical deformations of graphene flakes

The type I charged and doped graphene flakes, that have been geometrically optimized with the Def2TZVP and 6-31+G(2df, p) basis sets show very similar geometry. The root-mean-square deviation in Cartesian coordinates, after aligning two geometries obtained with different basis sets, using the Kabsch algorithm,[42] is about 0.01 Å. B and N dopants are known to be able to substitute the graphene's C atoms without significantly altering its geometry from the ideal honey-comb structure. Consistently, the B and N doping of the considered graphene flakes induces modest, but noticeable, alterations to the geometry of the graphene flakes.

Using the labelling scheme previously introduced in Fig. 2, we report in Fig 8 the relative bond length variations due to the dopants presence and to the loading or removal of an electron charge. The nearest-neighbour distances between the C_A carbons and the central atom are further specified in Table 2.

Table 2 Bond lengths (Å) for the carbons atom bonded to the flake's central atom in neutral type I flakes. Note that there are slight variations between the different ZA bonds in the neutral undoped flake since number of valence electrons of the central atom is four, implying that one of the C_A atoms (at the symmetry axis, column indicated with Z-A* below) connects to it via a double bond, while the other bonds (column Z-A) have the same length and reflect more a single bond character. In the doped charged isoelectric flakes this effect is also present. Overall, the effect seems to be reduced whenever the dopant provides an odd number of electrons to the flake. Moreover, the single/double bonds are switched whenever two electrons are added or removed from the isoelectric flakes.

Total charge	Bond Type	Z-A*	Z-A
$-1e$	C_Z-C_A	1.407	1.422
	B_Z-C_A	1.460	1.501
	N_Z-C_A	1.437	1.382
$0e$	C_Z-C_A	1.384	1.435
	B_Z-C_A	1.498	1.497
	N_Z-C_A	1.408	1.400
$+1e$	C_Z-C_A	1.411	1.420
	B_Z-C_A	1.534	1.484
	N_Z-C_A	1.358	1.419

N doping contracts the structure, B doping expands it. The bond length variation propagates consistently in the first and second neighbour, following an oscillatory decaying progression. The effects extends to the edges of the flake. The effects on the flakes bond length of the loaded charges are also reported in Fig 8. Beside the C_A atoms in the B-doped flakes, the added charges have modest effects on the geometrical structure of the flakes. A net $-1e$ charge results into a 1% contraction with respect to the C_A atoms of the neutral system.

Also note the variation between the distances of the central atom and its three nearest-neighbour atoms within a flake (Table 2). This variation is due to the double bond/single bond character of this connectivity. In the neutral undoped flake and the charged isoelectric doped flakes, the bond with the double bond character is always with the C_A atom at the symmetry line. The two other bonds, equal in size due to symmetry, have a single bond character. The single bond/double bond character is less dominantly present for neutral dopants and undoped charged flakes. Adding two electrons to the isoelectric B-dopant or removing two electrons from the isoelectric N-dopant show that single/double bonds switch.

5.2 Electric fields of neutral heterodoped type II flake

The heterodoping of N and B to the type II flake creates a permanent dipole and its magnitude can be computed by integrating out the full electron density. Table 3 reports the dipole moment and the quadrupole moments for a graphene type II flake, and the ones of a water molecule for comparison.

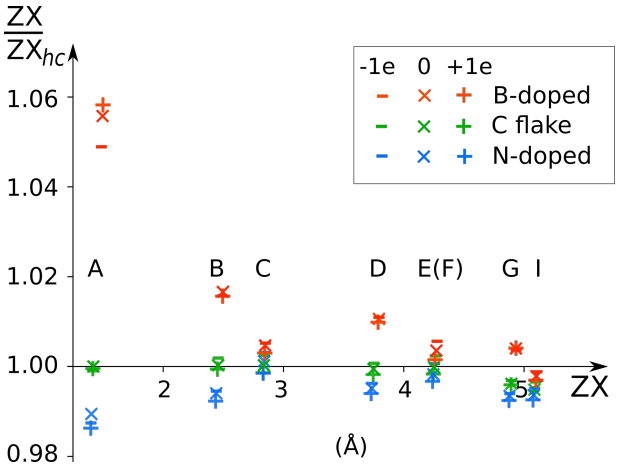

Fig. 8 Deviation from the honey-comb structure: distance between the central atom Z, ZX, and the groups of atoms C_A - C_I (See Fig. 2) divided by the corresponding distances in the ideal honeycomb structure ZX_{hc} with bond distances all equal to ZA of the neutral undoped flake. The central atom is either C, B or N, and the total charge is either $-1e$, $0e$, or $+1e$.

Table 3 Dipole moment (Debye), and Traceless Quadrupole moment components (Debye·Ang) for a type II flake and a water molecule.[43]

Multipole moments		Graphene flake	Water molecule
Dipole moment	d	1.32	1.85
Traceless	Θ_{XX}	23.66	2.323
Quadrupole	Θ_{YY}	21.56	-2.420
moment	Θ_{ZZ}	-45.22	0.097

It is also interesting to examine the effect of the heterodoping on the local electric field. Fig. 9 shows the electric field lines at the intersecting plane that crosses orthogonally the flake along the symmetry line. The lower panel, Fig. 9 shows the electrostatic field of singe water molecule for comparison.

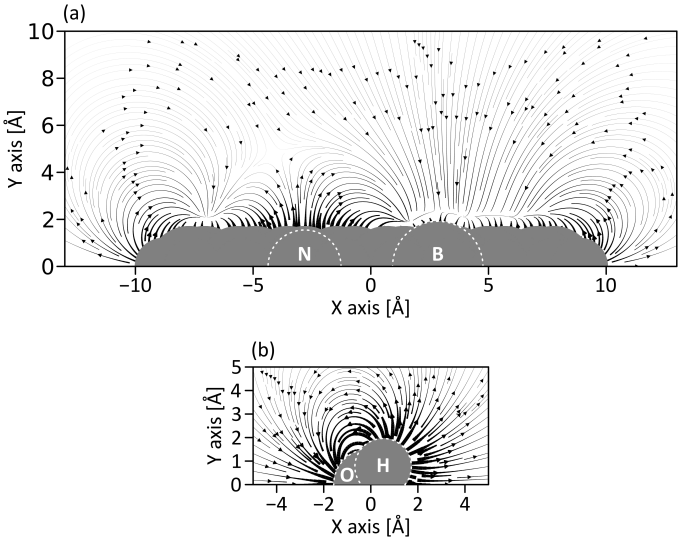

Fig. 9 Electrostatic field created (a) by the heterodoped graphene flake in the plane orthogonal to the flake through the long axis and (b) by a singe water molecule (for a visual comparison only). The strength of the electric field is proportional to the line thickness.

Taking into account the values for the multipole moments, reported in the Table 3, we can conclude, that the dipole moment for the type II flake is less then the one for the small water molecule, thus it cannot be controlled by the presence of the dopants. However, the electric field orthogonal to the flake is sensitive to the presence of dopants: quadrupole moments of the flake are an order of magnitude larger then the ones for water molecule. On Fig. 9 we can see that the field generated by the flake is modest in comparison with that of a water molecule. However, the field lines are clearly correlated to the presence of the dopants. Even though nitrogen bears a negative partial charge, the electric field is pointing away from this region because the neighbouring carbon atoms are positively charged, which is apparently the dominant effect in terms of the electric field.

6 Conclusions

The partial charges on graphene flakes have been quantified via two fundamentally different approaches: minimal-basis iterative stockholder (MBIS) method and restrained electron potential (RESP) fitted charges. The minimal-basis iterative stockholder, MBIS, has appeared as a more reliable method, providing a physically more consistent description.

The MBIS method has thus been applied to study the partial charges of the graphene flakes with a N and B dopant atoms located at the centre of the flakes. The system loaded or deprived of an electron has thereafter been studied reporting the relative capability of the system to react to external electric fields. Remarkably, we found that the B-dopant is mostly able to concentrate the local charges when an electron is added to the system.

Still, the accurate evaluation of the partial charges for large system requires a large computational cost due to the expensive DFT optimization procedure. The second-order atom-condensed Kohn-Sham DFT model (ACKS2) approach has been tuned to provide accurate results that are orders of magnitude faster than DFT.

The heterodoped graphene flake firstly demonstrates the possibility to construct, by design, a local electric field with tunable characteristics. The ACKS2 approach has been shown to represent an efficient and sufficiently reliable method to scan the large amount of degree of freedom to predict such fields. Furthermore, the partial charges of other analogues carbon materials, such as nanoribbons, fullerenes, and carbon nanotubes, can now be directly estimated via ACKS2.

Hence, this work has provided accurate partial charges for graphene based materials with the possible presence of dopants and net charges, The presented ACKS2 model permits automated high-throughput scans to map the effect of the system's constitutive variables. Combinations to obtain desired electric properties, such as atomic charges, dipoles and electric fields of interest, can readily be explored. As a result, the design of graphene interfaces with predefined characteristics, e.g. catalytic function,[44] becomes accessible, as well as the adsorption and reaction kinetic.[45,46] In addition, our approach can be adopted for other 2D materials, such as Molybdenum Disulfide (MoS2).[47,48]

Acknowledgements

AM, TSvE, and ER thank the Research Council of Norway for financial support (Proj. 237423 and 267669) and NOTUR for high-performance computing (NN9254K). T.V. acknowledges the Research Board of Ghent University (BOF) for its financial support.

References

1 K. Novoselov, A. Geim, S. Morozov, D. Jiang, Y. Zhang, S. Dubonos, I. Grigorieva and A. Firsov, *Science*, 2004, **306**, 666–669.

2 X.-K. Kong, C.-L. Chen and Q.-W. Chen, *Chem. Soc. Rev.*, 2014, **43**, 2841–2857.

3 D. Abergel, V. Apalkov, J. Berashevich, K. Ziegler and T. Chakraborty, *Adv. Phys.*, 2010, **59**, 261–482.

4 P. Avouris, *Nano Lett.*, 2010, **10**, 4285–4294.

5 S. Banerjee and D. Bhattacharyya, *Comput. Mater. Sci.*, 2008, **44**, 41–45.

6 D. Jiang and Z. Chen, *Graphene Chemistry: Theoretical Perspectives*, Wiley, 2013.

7 A. AlZahrani and G. Srivastava, *Appl. Surf. Sci.*, 2010, **256**, 5783–5788.

8 S. K. Singh, M. Neek-Amal and F. M. Peeters, *J. Chem. Phys.*, 2014, **140**, 074304.

9 B. Sanyal, O. Eriksson, U. Jansson and H. Grennberg, *Phys. Rev. B*, 2009, **79**, 113409.

10 S. Tang and Z. Cao, *J. Chem. Phys.*, 2011, **134**, 044710.

11 S. Chen, W. Cai, D. Chen, Y. Ren, X. Li, Y. Zhu, J. Kang and R. S. Ruoff, *New J. Phys.*, 2010, **12**, 125011.

12 A. Y. Mehandzhiyski, E. Riccardi, T. S. van Erp, T. T. Trinh and B. A. Grimes, *J. Phys. Chem. B*, 2015, **119**, 10710–10719.

13 O. Leenaerts, B. Partoens and F. M. Peeters, *Phys. Rev. B*, 2008, **77**, 125416.

14 A. AlZahrani, *Appl. Surf. Sci.*, 2010, **257**, 807–810.

15 G. R. Jenness, O. Karalti and K. D. Jordan, *Phys. Chem. Chem. Phys.*, 2010, **12**, 6375–6381.

16 M. Yang, A. Nurbawono, C. Zhang, Y. P. Feng and Ariando, *Appl. Phys. Lett.*, 2010, **96**, 193115.

17 A. Montoya, T. N. Truong and A. F. Sarofim, *J. Phys. Chem. A*, 2000, **104**, 6108–6110.

18 H. W. Zhang, Z. Q. Zhang and L. Wang, *Curr. Appl. Phys.*, 2009, **9**, 750–754.

19 J. Y. Chen, A. Kutana, C. P. Collier and K. P. Giapis, *Science*, 2005, **310**, 1480–1483.

20 M. Rahimi, J. K. Singh and F. Müller-Plathe, *J. Phys. Chem. C*, 2015, **119**, 15232–15239.

21 M. V. Fedorov and A. A. Kornyshev, *J. Phys. Chem. B*, 2008, **112**, 11868–11872.

22 F. Chiappini, S. Wiedmann, M. Titov, A. K. Geim, R. V. Gorbachev, E. Khestanova, A. Mishchenko, K. S. Novoselov, J. C. Maan and U. Zeitler, *Phys. Rev. B*, 2016, **94**, 085302.

23 E. Riccardi and A. I. Liapis, *J sep. sci.*, 2009, **32**, 4059–4068.

24 A. I. Liapis, E. Riccardi and J.-C. Wang, *J. sep. sci.*, 2010, **33**, 2749–2756.

25 T. Verstraelen, S. Vandenbrande, F. Heidar-Zadeh, L. Vanduyfhuys, V. Van Speybroeck, M. Waroquier and P. W. Ayers, *J. Chem. Theory Comput.*, 2016, **12**, 3894–3912.

26 C. I. Bayly, P. Cieplak, W. D. Cornell and P. A. Kollman, *J. Phys. Chem.*, 1993, **97**, 10269–10280.

27 W. J. Mortier, S. K. Ghosh and S. Shankar, *J. Am. Chem. Soc.*, 1986, **108**, 4315–4320.

28 T. Verstraelen, P. W. Ayers, V. V. Speybroeck and M. Waroquier, *J. Chem. Phys*, 2013.

29 T. Verstraelen, S. Vandenbrande and P. Ayers, *J. Chem. Phys.*, 2014, **141**, 194114.

30 W. L. Jorgensen, D. S. Maxwell and J. Tirado-Rives, *J. Am. Chem. Soc.*, 1996, **118**, 11225–11236.

31 T. Verstraelen, V. Van Speybroeck and M. Waroquier, *J. Chem. Phys.*, 2009, **131**, 044127.

32 L. Warren, J. Davis and S. Patel, *J. Chem. Phys.*, 2008, **128**, 144110.

33 R. a. Nistor, J. G. Polihronov, M. H. Müser and N. J. Mosey, *J. Chem. Phys.*, 2006, **125**, 94108.

34 G. A. Petersson, A. Bennett, T. G. Tensfeldt, M. A. Al-Laham, W. A. Shirley and J. Mantzaris, *J. Chem. Phys.*, 1988, **89**, 2193–2218.

35 F. Weigend and R. Ahlrichs, *Phys. Chem. Chem. Phys.*, 2005, **7**, 3297–3305.

36 S. Grimme, *J. Comput. Chem.*, 2006, **27**, 1787–1799.

37 M. J. Frisch, G. W. Trucks, H. B. Schlegel, G. E. Scuseria, M. A. Robb, J. R. Cheeseman, G. Scalmani, V. Barone, B. Mennucci, G. A. Petersson, H. Nakatsuji, M. Caricato, X. Li, H. P. Hratchian, A. F. Izmaylov, J. Bloino, G. Zheng, J. L. Sonnenberg, M. Hada, M. Ehara, K. Toyota, R. Fukuda, J. Hasegawa, M. Ishida, T. Nakajima, Y. Honda, O. Kitao, H. Nakai, T. Vreven, J. A. Montgomery, Jr., J. E. Peralta, F. Ogliaro, M. Bearpark, J. J. Heyd, E. Brothers, K. N. Kudin, V. N. Staroverov, R. Kobayashi, J. Normand, K. Raghavachari, A. Rendell, J. C. Burant, S. S. Iyengar, J. Tomasi, M. Cossi, N. Rega, J. M. Millam, M. Klene, J. E. Knox, J. B. Cross, V. Bakken, C. Adamo, J. Jaramillo, R. Gomperts, R. E. Stratmann, O. Yazyev, A. J. Austin, R. Cammi, C. Pomelli, J. W. Ochterski, R. L. Martin, K. Morokuma, V. G. Zakrzewski, G. A. Voth, P. Salvador, J. J. Dannenberg, S. Dapprich, A. D. Daniels, Ã. Farkas, J. B. Foresman, J. V. Ortiz, J. Cioslowski and D. J. Fox, *Gaussian09 Revision C.01*, Gaussian Inc. Wallingford CT 2009.

38 T. Verstraelen, P. Tecmer, F. Heidar-Zadeh, C. E. Gonzalez-Espinoza, M. Chan, T. D. Kim, K. Boguslawski, S. Fias, S. Vandenbrande, D. Berrocal and A. P. W., *HORTON 2.1.0*, Available via the Internet at: http://theochem.github.com/horton, accessed 23 Nov 2017.

39 E. Vanquelef, S. Simon, G. Marquant, E. Garcia, G. Klimerak, J. C. Delepine, P. Cieplak and F.-Y. Dupradeau, *Nucleic Acids Res.*, 2011, **39**, W511–W517.

40 Z. Zhou, X. Gao, J. Yan, D. Song and M. Morinaga, *Carbon*, 2004, **42**, 2677–2682.

41 P. Bultinck, S. Fias, C. Van Alsenoy, P. Ayers and R. Carbo-Dorca, *J. Chem. Phys.*, 2007, **127**, 34102.

42 W. Kabsch, *Acta Crystall. A*, 1978, **34**, 827–828.
43 J. Kongsted, A. Osted, K. V. Mikkelsen and O. Christiansen, *Chem. Phys. Lett.*, 2002, **364**, 379 – 386.
44 M. Moqadam, A. Lervik, E. Riccardi, V. Venkatraman, B. K. Alsberg and T. S. van Erp, *Proc. Natl. Acad. Sci. USA*, 2018, **115**, E4569–E4576.
45 T. S. van Erp, M. Moqadam, E. Riccardi and A. Lervik, *J. Chem. Theor. Comput.*, 2016, **12**, 5398–5410.
46 E. Riccardi, O. Dahlen and T. S. van Erp, *J. Phys. Chem. Lett.*, 2017, **8**, 4456–4460.
47 T. F. Jaramillo, K. P. Jørgensen, J. Bonde, J. H. Nielsen, S. Horch and I. Chorkendorff, *science*, 2007, **317**, 100–102.
48 B. Hinnemann, P. G. Moses, J. Bonde, K. P. Jørgensen, J. H. Nielsen, S. Horch, I. Chorkendorff and J. K. Nørskov, *Journal of the American Chemical Society*, 2005, **127**, 5308–5309.